Research Square

Preprints are preliminary reports that have not undergone peer review.
They should not be considered conclusive, used to inform clinical practice,
or referenced by the media as validated information.

Distinct Gut–Liver Adaptations to Dihydromyricetin and Silybin in Middle-aged Mice with Alcohol-associated Liver Injury

Jiajun Lei
Southern University of Science and Technology
Xinyi Zeng
Sirio Life Technology Co., Ltd
Lisha Liang
Southern University of Science and Technology
Xingkun Ji
Southern University of Science and Technology
Yuepu Zhao
Sirio Life Technology Co., Ltd
Cuishan Huang
Chinese Academy of Sciences
Danyang Yu
Sirio Life Technology Co., Ltd
Quancai Sun
Macau University of Science and Technology
Xinluan Wang
Chinese Academy of Sciences
Jian-Kang Zhu
Southern University of Science and Technology
Yu-Xuan Lyu
lvyx@sustech.edu.cn

Southern University of Science and Technology

Article

Keywords: Alcohol-associated liver disease (ALD), Gut–liver axis, Multi-omics, Dihydromyricetin, Silybin, Aging

Posted Date: July 20th, 2026

DOI: https://doi.org/10.21203/rs.3.rs-10253659/v1

License: This work is licensed under a Creative Commons Attribution 4.0 International License.
Read Full License

Additional Declarations: No competing interests reported.

Version of Record: A version of this preprint was published at npj Aging on October 3rd, 2026. See the published version at https://doi.org/10.1038/s41514-026-00528-w.

Abstract

Alcohol-associated liver disease (ALD) is increasingly recognized as an age-related systemic disorder shaped by gut–liver axis dysfunction, yet how ageing influences disease susceptibility and intervention responses remains poorly understood. By integrating GBD and NHANES data, we identified middle age as a critical window of heightened alcohol-associated hepatic vulnerability and modeled this context in 11–12-month-old male mice. We compared Dihydromyricetin (DHM) and Silybin to determine whether these bioactive interventions elicit distinct gut–liver axis adaptations under middle-aged alcohol exposure. Both interventions partially attenuated alcohol-associated mortality and hepatic steatosis, whereas conventional serum biochemical responses were modest and endpoint-dependent. Multi-omics profiling revealed this overlapping phenotypic protection arose from divergent adaptive trajectories. DHM was associated with adaptive energy metabolism, detoxification-associated remodeling, jejunal epithelial renewal, and host-state-dependent microbial remodeling, including context-dependent regulation of *Akkermansia*. In contrast, Silybin aligned with proteostatic stress buffering, inflammatory lipid regulation, and immune-associated ecological rebalancing. These findings demonstrate that the host's physiological state critically shapes intervention outcomes. By defining distinct metabolic–epithelial–microbial adaptation patterns in middle-aged ALD, this study provides a rationale for age-stratified intervention strategies in aging-associated liver injury.

Introduction

Alcohol-associated liver disease (ALD) is one of the leading drivers of chronic liver disease mortality worldwide[1,2]. The pathogenesis of ALD encompasses a broad and progressive histological spectrum, initiating with simple hepatic steatosis and advancing to alcohol-associated steatohepatitis (ASH), progressive fibrosis, cirrhosis and ultimately hepatocellular carcinoma[3]. This progression is driven by acetaldehyde toxicity, redox imbalance, induction of cytochrome P450 2E1 (CYP2E1), mitochondrial dysfunction and disordered lipid metabolism[3,4]. Crucially, the global burden of ALD has continued to rise in recent years, reflecting the cumulative nature of long-term, high-risk drinking behaviors and underscoring an urgent clinical need to identify susceptibility windows[2,5]. Consequently, there is a pressing demand to develop safe, long-term intervention strategies tailored to age-related physiological vulnerability[1,2,5]. Because alcohol-associated hepatic injury is linked to long-term lifestyle exposure and systemic metabolic stress, interventions with favorable safety profiles and multi-target regulatory properties may be particularly relevant for at-risk populations.

Historically, ALD was viewed as a consequence of local hepatic pathology driven primarily by the toxic byproducts of ethanol metabolism. However, this paradigm has fundamentally shifted. Accumulating evidence now positions ALD as a profound systemic disorder mediated by the bidirectional communication of the gut-liver axis[6,7]. Chronic ethanol consumption directly compromises the intestinal epithelial barrier and increases gut permeability. This “leaky gut” phenotype precipitates microbial dysbiosis and facilitates the translocation of bacterial endotoxins and pro-inflammatory mediators into

the portal circulation. Upon reaching the liver, gut-derived pathogen-associated molecular patterns (PAMPs), particularly lipopolysaccharide (LPS), activate Kupffer-cell TLR4 signaling and trigger a cascade of pro-inflammatory cytokines, including TNF-α and IL-6[8,9]. This gut-derived inflammatory influx amplifies hepatic inflammation and metabolic injury, positioning the gut–liver axis as the critical nexus for ALD progression and a prime target for system-level, age-relevant interventions[6,10]. Therefore, interventions targeting alcohol-associated liver injury should not be evaluated solely by conventional hepatocellular injury markers, but should also account for intestinal barrier adaptation, microbial ecology and systemic metabolic remodeling.

Despite this systemic understanding, physiological age remains a profoundly underestimated variable in preclinical ALD research. Clinically, alcohol-associated liver injury often shows cumulative, age-dependent pathogenesis[2,11,12]. However, the vast majority of experimental ALD studies rely on young rodents. Because young animals possess robust regenerative capacities and resilient microbial ecosystems, they fail to capture the vulnerabilities of the primary clinical demographic. Middle age represents a critical biological inflection point characterized by declining intestinal barrier function, altered immune homeostasis, reduced mitochondrial capacity, and attenuated tissue repair[13–15]. Preclinical evidence increasingly demonstrates that this age-related physiological decline exacerbates alcohol-induced intestinal barrier disruption, hepatic inflammation, and susceptibility to acute-on-chronic liver injury[11,12,16]. Consequently, middle-aged animal models are essential for capturing age-related vulnerability in alcohol-associated liver injury. This requirement is especially important for evaluating interventions whose effects depend on the host's baseline metabolic, immune and microbial state. A compound that successfully protects a young liver may produce substantially different effects in a middle-aged, metabolically compromised context. Thus, age-relevant models are essential for defining how interventions reshape systemic adaptation in susceptible hosts exposed to chronic alcohol-related metabolic stress.

DHM and Silybin are two widely studied naturally derived bioactive compounds with reported hepatoprotective and metabolic regulatory activities. DHM is a flavonoid enriched in vine tea (*Nekemias grossedentata*), whereas Silybin is the major bioactive flavonolignan from milk thistle (*Silybum marianum*). Previous studies suggest that these compounds have hepatoprotective and metabolic regulatory activities, including effects on hepatic lipid accumulation, inflammatory responses and mitochondrial dysfunction [17,18]. However, most studies have evaluated these compounds separately, often in young animals or simplified injury models, leaving unclear whether they engage shared or distinct adaptive programs under age-related physiological vulnerability. If two bioactive interventions improve similar physiological endpoints but utilize divergent systemic regulatory paths, they should not be treated as mechanistically interchangeable. Their value should not be judged solely by isolated endpoints such as ALT, AST, or hepatic lipid deposition. Instead, an integrated analysis encompassing hepatic pathology, systemic metabolism, intestinal responses and microbial ecology may help define how different bioactive interventions reshape systemic adaptation under age-related vulnerability. Such

systems-level information is essential for understanding how age-related physiological state shapes intervention responses in ALD.

To address these translational gaps, we first integrated population-level data from Global Burden of Disease (GBD) and National Health and Nutrition Examination Survey (NHANES) databases to establish middle age as a high-susceptibility window for alcohol-associated liver injury. Guided by these epidemiological insights, we established a clinically relevant model of chronic alcohol-associated liver injury utilizing male C57BL/6J mice at 11–12 months of age, broadly modeling a middle-aged physiological state. Within this framework, we systematically compared DHM with Silybin, a well-established hepatoprotective reference compound, by integrating assessments of mortality, hepatic and intestinal pathology, with a comprehensive multi-omics approach, encompassing hepatic and jejunal transcriptomics, serum metabolomics, and 16S rRNA microbial profiling. Crucially, our primary objective was not merely to determine which compound exhibited superior hepatoprotection. Rather, we sought to elucidate whether these two bioactive interventions elicit divergent molecular, metabolic, and ecological adaptations across the gut–liver axis under middle-aged alcohol-associated liver injury. By mapping these distinct adaptive routes, our work provides systems-level evidence that middle-aged physiology shapes gut–liver axis responses to bioactive interventions in alcohol-associated liver injury.

Results

Multi-cohort Epidemiological Evidence Identifies Middle Age as a Critical Window of Susceptibility to Alcohol-Associated Hepatic Stress

To establish the clinical rationale for our study, we first evaluated population-level datasets to determine how physiological age influences susceptibility to alcohol-associated liver disease (ALD). Analysis of the Global Burden of Disease (GBD) database showed that ALD prevalence increased non-linearly with age and peaked at 50–70 years, with a pronounced male bias (**Fig. 1A**). This trajectory implies that the cumulative hepatic burden of chronic alcohol exposure manifests most severely during middle age.

To further investigate this age-dependent vulnerability, we analyzed cross-sectional data from the NHANES cohorts. Continuous variable regression confirmed that the dose-response slope between alcohol intake and GGT elevation was markedly steeper in the middle-aged strata, indicating that physiological aging exacerbates alcohol-induced hepatic stress (**Fig. 1B**). Under comparable intensities of alcohol consumption, middle-aged individuals (35–49 and 50–64 years) exhibited substantially higher serum liver injury markers (GGT, AST and ALT) compared to younger cohorts (18–34 years), with GGT showing the most acute sensitivity to both age and drinking exposure (**Fig. 1C–E**). The subsequent decline in these markers within the senior cohort (≥65 years) likely reflects survivor bias or health-related drinking cessation.

DHM and Silybin Confer Partial Protection Against Alcohol-Associated Mortality and Liver Pathology in Middle-Aged Mice

Based on these human epidemiological findings, we selected 11–12-month-old male C57BL/6J mice, an age range commonly classified as middle-aged in laboratory mice [20], to construct a chronic alcohol-associated liver injury model (**Fig. 2A**). Over the course of the experimental period, chronic alcohol feeding markedly reduced survival in the EtOH group. Conversely, DHM and Silybin attenuated this alcohol-induced mortality (**Fig. 2B**). Body weight and food intake were monitored throughout the intervention period, and the pair-fed design helped minimize confounding effects caused by differences in caloric intake **(Fig. S1A,B)**.

At the endpoint, chronic alcohol exposure produced a robust hepatic injury phenotype, as reflected by increased liver/body weight ratio and altered serum biochemical readouts **(Fig. 2C–F)**, and pronounced hepatic lipid accumulation and steatosis in Oil Red O and H&E staining (**Fig. 2G–J**). These findings confirmed that the alcohol-feeding protocol successfully induced key pathological features of alcohol-associated liver injury in a middle-aged physiological context.

In contrast to the profound injury induced by alcohol, the phenotypic effects of DHM and Silybin on conventional hepatic endpoints were modest and endpoint-dependent. Neither intervention significantly normalized the liver/body weight ratio, serum AST, ALT, or TG levels across all comparisons (**Fig. 2C–F**), although DHM did show a trend toward reduced ALT. Histological assessment revealed a partial attenuation of alcohol-associated lipid deposition. Silybin showed a significant reduction in Oil Red O-positive area and a downward trend in steatosis area, whereas DHM produced a milder histological improvement (**Fig. 2G–J**). Together, these data indicate that DHM and Silybin did not produce a uniform biochemical reversal of alcohol-induced liver injury, but instead conferred partial and partially overlapping phenotypic protection. This nuanced macroscopic outcome prompted us to further examine whether these two compounds engage distinct molecular, metabolic and intestinal regulatory programs that extend beyond conventional liver injury readouts.

DHM and Silybin Interventions Exhibit Favorable Safety Profiles in Middle-Aged Mice

To verify the safety profiles of these interventions, we evaluated markers of systemic toxicity. Histological examination of renal tissues revealed intact parenchymal architecture across all groups, with no marked glomerular atrophy, tubular dilation, or interstitial inflammatory cell infiltration in either alcohol-exposed or intervention groups (**Fig. S1C**). These findings suggest that the doses used did not induce overt histological nephrotoxicity under the present experimental conditions. Furthermore, the

spleen index remained stable across all groups, indicating the absence of gross peripheral immune organ hypertrophy (**Fig. S1D**).

Beyond hepatic and systemic organ parameters, we assessed the impact of these interventions on physical function and behavior. Neither DHM nor Silybin exhibited adverse effects on systemic functional responses, with mice showing no significant deficits in grip strength or general open-field testing. Notably, the only functional deviation observed was in the open-field test, where DHM administration alone significantly increased total ambulatory distance (**Fig. S1E,F**), suggesting a potential mild stimulatory effect on baseline locomotor activity rather than a deficit. Together, these findings demonstrate that neither bioactive intervention produced overt renal, splenic, or behavioral toxicity under the present experimental conditions.

Hepatic Transcriptomic Profiling Reveals Distinct Molecular Responses to DHM and Silybin in Middle-Aged Alcohol-Fed Mice

To further elucidate the regulatory mechanisms of DHM and Silybin in middle-aged alcohol-associated liver injury, we performed transcriptomic profiling of liver tissues. Hepatic transcriptomics showed that chronic alcohol exposure broadly remodeled liver gene expression (**Fig. S2A–E**). Supplementary GSEA analyses, including ribosome-related and additional compound-associated pathways, are shown in **Fig. S2F–K**. Although DHM and Silybin did not fully segregate from the EtOH group in principal component analysis (PCA) space, differential gene expression analysis revealed distinct regulatory trajectories. Notably, DHM (80 DEGs) and Silybin (77 DEGs) shared only 12 overlapping genes (**Fig. 3A**), indicating that these compounds acted through distinct and minimally overlapping regulatory programs.

Gene Set Enrichment Analysis (GSEA) first revealed divergent pathway-level responses. DHM intervention drove a positive enrichment of oxidative phosphorylation and thermogenesis, indicating an adaptive energy-metabolic transcriptional response (**Fig. 3B**). This transcriptional signature aligned with the increased locomotor activity trend observed in behavioral testing (**Fig. S1F**) , suggesting that DHM may enhance metabolic adaptive capacity under alcohol-induced stress. Conversely, Silybin was associated with negative enrichment of primary bile acid biosynthesis and citrate cycle (TCA cycle) pathways (**Fig. 3C,D**), implying that it may reduce selected metabolic loads and lipid-related stress during alcohol-associated hepatic injury. Hierarchical GO enrichment further distinguished the functional programs of the two interventions: DHM was associated with vascular and transport-related processes **(Fig. 3E)**, whereas Silybin preferentially enriched proteostasis- and stress-buffering-related pathways, including protein folding, protein processing in endoplasmic reticulum and endoplasmic reticulum unfolded protein response (ER UPR) **(Fig. 3F; Fig. S2K)**.

Although the two interventions showed divergent regulatory directions, they also exhibited shared protective features. GSEA demonstrated that chronic alcohol exposure markedly suppressed the

ribosome pathway, whereas both DHM and Silybin partially restored this translation-related process (**Fig. S2F**–**H**). The maintenance of basal protein synthesis capacity may therefore represent a core, shared protective feature of both interventions.

Taken together, hepatic transcriptomic profiling indicates that while DHM and Silybin did not fully reverse the global alcohol-associated transcriptional imbalance, they orchestrate distinct molecular response patterns. DHM is characterized by adaptive metabolic remodeling, while Silybin drives stress-buffering regulation, both of which may contribute to mitigating middle-aged alcohol-associated liver injury.

Serum Metabolomics Identifies Divergent Systemic Metabolic Remodeling Induced by DHM and Silybin in Middle-Aged Alcohol-Fed Mice

To delineate how DHM and Silybin modulate systemic metabolism in the middle-aged alcohol-associated liver injury model, we performed untargeted serum metabolomics. Quality control and differential metabolite screening are shown in **Fig. S3A–D**. PCA and Orthogonal Projections to Latent Structures Discriminant Analysis (OPLS-DA) showed that chronic alcohol exposure markedly shifted the serum metabolomic landscape, while DHM and Silybin interventions induced distinct metabolic remodeling patterns (**Fig. 4A,B; Fig. S3E**). Notably, the EtOH+DHM group clustered closer to the Control and DHM-only groups and segregated away from the EtOH group in the ordination space, suggesting that DHM buffered alcohol-associated global metabolic disruption.

Differentially abundant metabolite (DAM) analysis further underscored the pronounced divergence in systemic metabolic regulation. Compared with the EtOH group, DHM intervention yielded 23 DAMs, whereas Silybin yielded 48 DAMs, with the two interventions sharing only one overlapping metabolite (**Fig. 4C**). This stark separation confirms that these bioactives engage different metabolic regulatory trajectories in the middle-aged ALD context. KEGG enrichment and compound-pathway network analyses further revealed functional biases between the two interventions. The DHM group exhibited significant enrichment in the metabolism of xenobiotics by cytochrome P450 pathway, with S-(Formylmethyl)glutathione as a central hub (**Fig. 4D,E**). In contrast, Silybin orchestrated a broader remodeling of lipid metabolism and inflammation-associated pathways. Its metabolic network centered on arachidonate as a highly connected hub (**Fig. 4F**).

As a glutathione-conjugated product linked to acetaldehyde metabolism, the change in S-(Formylmethyl) glutathione (**Fig. 4G**) implies that DHM-induced metabolic remodeling involves detoxification and transport of alcohol-related toxic metabolites. This metabolic feature corroborates the enhanced oxidative phosphorylation observed in the hepatic transcriptome, reinforcing the hypothesis that DHM buffers alcohol-associated systemic stress by strengthening metabolic adaptation. Conversely, Silybin reduced arachidonic acid levels (**Fig. 4H**), indicating preferential regulation of inflammatory lipid signaling and metabolic homeostatic recovery. Furthermore, Silybin markedly altered levels of D-Alanyl-

D-alanine and biotin (**Fig. 4I,J**). Given that these metabolites are linked to microbial metabolic activity, this result suggests that the protective effects of Silybin may involve gut microbiota-associated metabolic alterations.

Despite this overarching metabolic divergence, DHM and Silybin also shared specific metabolic features. For example, both interventions significantly attenuated the alcohol-associated increase in 1-O-(11-hydroxyoleoyl)-sn-glycero-3-phosphocholine (**Fig. 4K**), suggesting a shared capacity to alleviate alcohol-associated membrane lipid metabolic disruption. GSEA further showed that DHM preferentially enriched bile secretion-related pathways (**Fig. S3F**), whereas Silybin modulated broader systemic metabolic pathways (**Fig. S3G**). These findings further support the distinct yet partially complementary characteristics of the two interventions at the level of systemic metabolic regulation.

Together, serum metabolomics indicates that DHM and Silybin drive differential metabolic remodeling patterns in the middle-aged ALD context. DHM is characterized by metabolic detoxification adaptation, whereas Silybin governs lipid-inflammatory regulation, with both distinct patterns ultimately mitigating alcohol-associated systemic metabolic disruption.

Jejunal Transcriptomics Reveals Divergent Barrier Defense Strategies Centered on *Sgk1* and *Rhobtb1*

As the first major contact site for alcohol and its metabolites, the jejunal barrier is critical for limiting alcohol-associated systemic injury. We therefore performed transcriptomic analysis of jejunal tissues to define how DHM and Silybin differentially regulate the gut–liver axis. PCA showed that chronic alcohol exposure markedly altered the global jejunal transcriptomic landscape in middle-aged mice, while DHM and Silybin induced transcriptional remodeling in different directions (**Fig. 5A**). Differential gene expression analysis further highlighted these divergent jejunal regulatory spectra: DHM and Silybin each regulated numerous distinct genes with limited overlap (**Fig. 5B**). This suggests that the two bioactives use different protective strategies for intestinal barrier adaptation. To resolve these divergent jejunal responses, we organized the downstream analyses into paired functional modules, including GSEA pathways (**Fig. 5C,D**), retinol- and cell-cycle-related heatmaps (**Fig. 5E,F**), GO enrichment (**Fig. 5G,H**) and PPI networks (**Fig. 5I,J**).Supplementary volcano plots, alcohol-induced pathway changes, global heatmap, additional GSEA analyses and RT-qPCR validation are provided in **Fig. S4A–N**. Further pathway analyses showed that alcohol exposure hyperactivated stress- and xenobiotic metabolism-related pathways, including drug metabolism–cytochrome P450, chemical carcinogenesis and retinol metabolism (**Fig. S4D,F,I,J**). Concurrently, basal metabolic processes, such as ribosome and oxidative phosphorylation pathways, were suppressed (**Fig. S4F,H**). The middle-aged jejunum therefore appeared to enter a state of metabolic and stress disequilibrium under chronic alcohol stimulation.

In this alcohol-induced injury context, DHM preferentially drove adaptive repair and regeneration programs. GSEA showed an enrichment of cell cycle and DNA replication pathways in the DHM group

(**Fig. 5C; Fig. S4G**), while the cell-cycle-related heatmap further illustrated coordinated expression changes in representative genes **(Fig. 5F)**, suggesting partial recovery of alcohol-suppressed intestinal regenerative programs. This was confirmed by RT-qPCR, which demonstrated that DHM partially reversed the alcohol-induced upregulation of the cell cycle arrest gene *Cdkn1a* (**Fig. S4M**). GO enrichment further showed that DHM-associated DEGs were enriched for amino acid transport, response to peptide hormone and antibacterial humoral response (**Fig. 5G**). Protein-protein interaction (PPI) network analysis identified *Sgk1*, a kinase critical for epithelial stress adaptation and transport regulation, as a key node in the DHM-regulated network (**Fig. 5I**). *Sgk1* expression was elevated by alcohol and was partly normalized by DHM (**Fig. S4L**), suggesting that DHM fine-tunes epithelial stress adaptation and nutrient transport. Furthermore, DHM partially restored the expression of the antimicrobial defense gene *Reg3g* (**Fig. S4N**), maintaining epithelial innate immune integrity under alcohol stress.

Conversely, Silybin preferentially orchestrated detoxification and immune-homeostatic programs. GSEA showed that Silybin significantly suppressed the drug metabolism–cytochrome P450 pathway (**Fig. 5D**), while GO enrichment revealed pronounced immune-associated signatures, including response to bacterium, MDA-5, RIG-I and interleukin-27-mediated signaling pathways (**Fig. 5H**). Furthermore, both bioactives partially reversed the aberrant activation of retinol metabolism genes induced by alcohol, though the DHM-mediated recovery more closely approximated the baseline control state (**Fig. 5E**). PPI network analysis further identified *Rhobtb1* as a core node in the Silybin-regulated network (**Fig. 5J**). RT-qPCR showed that *Rhobtb1* increased significantly after alcohol exposure, whereas DHM and Silybin both reduced its expression (**Fig. S4K**). This suggests that *Rhobtb1* may participate in alcohol-associated jejunal stress remodeling.

Taken together, jejunal transcriptomic analysis demonstrates that DHM and Silybin initiated distinct intestinal adaptive programs under middle-aged alcohol exposure. DHM preferentially promoted epithelial adaptive repair, regeneration and transport-related processes, whereas Silybin preferentially regulated detoxification and immune-homeostatic programs. This divergent intestinal regulation may contribute to differences in the systemic protective effects of the two bioactives.

DHM and Silybin Differentially Reshape Gut Microbial Ecology in Middle-Aged Alcohol-Fed Mice

Because the gut microbiota serves as the critical ecological hub linking intestinal transcriptional adaptation, systemic metabolic remodeling, and liver injury, we performed 16S rRNA microbiome sequencing to elucidate how DHM and Silybin differentially regulate the middle-aged gut–liver axis. Principal Coordinate Analysis (PCoA) showed that chronic alcohol exposure markedly restructured the global gut microbial architecture (**Fig. 6A**). Both DHM and Silybin partly shifted this alcohol-associated microbial structure back toward the Control state, with the EtOH+DHM group aligning closer to the Control group along PC1. However, genus-level community composition analysis showed that while both

compounds alleviated alcohol-induced dysbiosis, their core microbial remodeling patterns were distinct (**Fig. 6B,C**).

Contribution analysis demonstrated that DHM and Silybin converged on partially shared ecological nodes, such as *Akkermansia*, *Faecalibaculum*, *Muribaculaceae* and *Lachnospiraceae NK4A136 group*, but their regulatory directions differed, as shown by the DHM-associated contribution profile **(Fig. 6D)**. This implies that rather than targeting entirely separate microbial populations, these two bioactives impose distinct remodeling effects on shared ecological nodes, thereby generating divergent microbial trajectories.

Notably, DHM showed a marked, context-dependent microbial remodeling capacity. By constructing a dual-coordinate ecological response map comparing the basal DHM response to the alcohol-stressed DHM response, we observed that many dominant response genera localized to quadrants II and IV, indicating diametrically opposed DHM responses depending on the host's stress state (**Fig. 6E**). Seven of the top 10 abundant response genera, including *Faecalibaculum*, *Akkermansia*, *Ligilactobacillus* and *Romboutsia*, exhibited this behavior (**Fig. 6E**). For example, *Faecalibaculum* was suppressed by DHM under basal conditions but re-enriched under alcohol exposure, whereas *Akkermansia* was enriched by DHM under normal conditions but decreased under alcohol stress. This bidirectional ecological response strongly suggests that DHM dynamically recalibrates microbial homeostasis in response to the host's metabolic state, rather than unidirectionally promoting selected "beneficial" taxa. For comparison, the corresponding Silybin-associated contribution profile further illustrated a distinct set of contributing genera **(Fig. 6F)**.

Supplementary diversity, phylum-level composition and LEfSe analyses are shown in **Fig. S5A–G**. Further genus-level quantification supported these trends (**Fig. S5H–K**). Chronic alcohol exposure expanded *Escherichia-Shigella*, whereas DHM intervention reduced its abundance (**Fig. S5K**). Concurrently, *Lachnospiraceae NK4A136 group* was relatively enriched after DHM intervention (**Fig. S5J**). Together with the hepatic transcriptomic, serum metabolomic and jejunal transcriptomic data, these microbial shifts confirm the existence of distinct system-level regulatory logic within the middle-aged gut–liver axis. Ultimately, DHM preferentially drives adaptive ecological remodeling, whereas Silybin orchestrates a pattern more consistent with inflammation-associated ecological rebalancing.

Discussion

Alcohol-associated liver disease (ALD) has historically been viewed as a localized hepatic disorder driven by ethanol metabolism, oxidative stress, lipid deposition and inflammation. Ethanol metabolism fundamentally alters hepatocellular redox status, induces CYP2E1 expression and amplifies reactive oxygen species generation, thereby precipitating steatosis, inflammatory responses and hepatocellular injury [21–23]. However, accumulating evidence indicates that ALD is not simply a liver-restricted pathology. It is a profound systemic disorder intricately linked to intestinal barrier integrity, microbial ecology, systemic metabolism, and the host's age-related physiological state. Chronic alcohol exposure severely

disrupts gut microbial composition and intestinal barrier integrity, increasing the influx of gut-derived inflammatory signals into the portal circulation and amplifying hepatic immune metabolic injury. Consequently, the gut–liver axis has emerged as a central framework for ALD research [7]. Within this context, our objective was not to frame DHM and Silybin as competing hepatoprotective compounds to be ranked by efficacy. Instead, we utilized the clinically relevant, high-susceptibility window of middle-aged ALD to systematically decode their differential regulatory trajectories across the gut–liver axis. Overall, our data indicate that DHM and Silybin produced partially overlapping phenotypic protection but engaged distinct adaptive routes: DHM preferentially aligned with metabolic–epithelial–microbial adaptation, whereas Silybin was more closely associated with stress buffering, inflammatory lipid regulation and immune-associated ecological rebalancing.

A primary implication of this study is that host age must be formally incorporated into the logic of intervention strategies for ALD. While the vast majority of experimental ALD studies rely on young mice, clinical alcohol-associated hepatic injury is cumulative and age-dependent. Our GBD analysis demonstrated that the 35–49 and 50–64-year demographic strata exhibit stronger liver enzyme responses under comparable drinking intensities, providing a robust clinical rationale for the use of mice at 11–12 months of age. Furthermore, because our epidemiological data revealed that males exhibit a higher prevalence and a steeper age-related spike in ALD burden (**Figure 1A**), we utilized male mice to model this higher-risk epidemiological context. Middle-aged physiology is intrinsically accompanied by reduced barrier function, altered immune homeostasis, lower metabolic flexibility and diminished tissue repair capacity[13–15]. These factors may amplify gut–liver axis injury during chronic alcohol exposure. For bioactive interventions in aging-associated ALD, this distinction is critical because their effects do not operate uniformly across physiological stages. Their protective effects depend on host metabolic state, gut microbial ecology, and tissue repair capacity. By focusing on middle-aged ALD, this study bridges a critical translational gap and provides experimental support for age-relevant evaluation of bioactive compounds in alcohol-associated liver injury[12].

At the phenotypic level, DHM and Silybin delayed alcohol-associated mortality and partially attenuated selected histological features of hepatic lipid deposition, although their effects on conventional biochemical markers were modest and endpoint-dependent. This is consistent with previous reports of the hepatoprotective potential of these compounds [18,24]. The more important finding, however, is not simply that both were effective. Rather, similar protective phenotypes were driven by different system-level regulatory logic. Historically, natural product research often places polyphenols and flavonoids into a unified antioxidant or anti-inflammatory framework. However, our integrated transcriptomic and serum metabolomic data suggest that under middle-aged alcohol stress, DHM and Silybin do not converge on a singular protective pathway. Instead, they deploy distinct adaptive strategies.

DHM-associated changes were predominantly concentrated in energy-metabolic adaptation and handling of exogenous toxic metabolites. Enrichment of hepatic oxidative phosphorylation and thermogenesis pathways, together with serum xenobiotic metabolism by cytochrome P450 and S-(Formylmethyl)glutathione-associated networks, suggests that DHM may preferentially enhance

adaptive metabolic capacity under alcohol-related metabolic pressure. This pattern is consistent with reports that DHM can influence lipid metabolism, mitochondrial bioenergetics and metabolic signaling[24]. It also provides a more specific interpretive framework than antioxidant activity alone. Importantly, this study did not directly measure mitochondrial respiration, CYP activity or glutathione metabolic flux. The DHM signature should therefore be interpreted as a network-level adaptive metabolic feature rather than a validated direct mechanism.

Conversely, Silybin appeared to reduce cellular stress load and limit expansion of inflammatory lipid signaling. Its hepatic transcriptional response was concentrated in protein folding, ER protein processing and ER UPR pathways, whereas serum metabolomics showed arachidonic acid-associated changes. These patterns suggest that Silybin may contribute to remodeling of inflammatory lipid pathways. Given that ER stress, UPR and arachidonic acid metabolism are closely linked to chronic liver disease and alcohol-associated inflammatory injury[25–29], Silybin in this model is better understood as a stress-buffering modulator than as a simple antioxidant. Therefore, DHM and Silybin are not interchangeable; rather, they represent two distinct bioactive intervention modes: enhanced metabolic adaptation versus stress-inflammatory buffering.

A notable finding was the association of DHM and Silybin with distinct candidate regulatory nodes in the jejunum, among which *Sgk1* and *Rhobtb1* deserve particular attention. SGK1 is a stress-responsive serine/threonine kinase involved in ion transport, nutrient absorption, cell survival and metabolic adaptation. Previous studies show that SGK1 can regulate intestinal Na^+-coupled glucose transporter 1 (SGLT1) and Na^+/H^+ exchanger 3 (NHE3), suggesting close links to intestinal epithelial transport and nutrient absorption[30–33]. Here, DHM-associated jejunal transcriptional changes were accompanied by amino acid transport, cell cycle/DNA replication, *Cdkn1a* downregulation and partial *Reg3g* recovery. These findings suggest that DHM may act beyond the liver and may involve remodeling of jejunal epithelial stress adaptation, nutrient transport and epithelial renewal programs. While our current data do not establish SGK1as a direct functional target, they provide a useful putative entry point for exploring a bioactive-driven “intestinal epithelial transport-systemic metabolic adaptation” axis.

Similarly, RHOBTB1 emerged as a candidate node in the Silybin-associated stress-buffering network. Existing studies have mainly examined RHOBTB1 in the vascular system, where it is linked to PPARγ-associated protection, oxidative stress and inflammatory regulation. RHOBTB1 is considered a downstream target of PPARγ and participates in maintaining vascular function while suppressing oxidative stress and inflammation-associated injury[34–36]. Although little is known about RHOBTB1 in intestinal epithelium or ALD, this makes it a potentially valuable candidate node. In this study, alcohol exposure significantly induced *Rhobtb1*, whereas DHM and Silybin both reduced its expression. For Silybin, the emergence of *Rhobtb1* alongside immune-associated pathways, ER stress buffering and inflammatory lipid metabolism suggests that it may participate in alcohol-associated jejunal stress remodeling. Future work using intestinal organoids, siRNA or CRISPR perturbation, or intestinal epithelial-specific animal models is warranted to test the functional significance of RHOBTB1 under alcohol stress.

Beyond their divergent pathways, the shared regulation of retinol metabolism represents a critical convergent node linking alcohol exposure, epithelial homeostasis and age-related metabolic vulnerability. Long-term alcohol intake is closely associated with disruption of vitamin A and retinoid metabolism. Ethanol can interfere with retinoid signaling and vitamin A homeostasis by sharing metabolic enzyme systems with retinol and by promoting CYP2E1-mediated retinoic acid catabolism[37–39]. Retinoid metabolism is linked not only to hepatic lipid metabolism, but also to immune regulation and epithelial homeostasis[40,41]. In the jejunal transcriptome, alcohol exposure markedly activated retinol metabolism-related genes, whereas DHM and Silybin both partly prevented this abnormal activation. DHM shifted the pattern closer to the control state. Retinoid metabolic homeostasis may therefore represent a shared metabolic node linking alcohol exposure, intestinal epithelial state and bioactive intervention.

The microbiome results further highlight the host-state dependency of intervention responses in middle-aged ALD. Many studies show bidirectional interactions between dietary polyphenols and the gut microbiota: polyphenols can alter microbial composition and metabolic function, whereas the microbiota determines polyphenol transformation, bioavailability and host response [42–44]. This means that the same bioactive compound may produce different, or even opposite, ecological consequences across host states. The DHM quadrant map captured this state dependency. High-abundance response genera such as *Akkermansia*, *Faecalibaculum*, *Ligilactobacillus* and *Romboutsia* changed in opposite directions under basal and alcohol-stressed states. This indicates that DHM does not simply act as a unidirectional prebiotic; rather, it drives context-dependent microbial remodeling.

Akkermansia provides a useful example of this context-dependent ecological response[45]. *A. muciniphila* is a commensal mucin-degrading bacterium commonly found in the human gut microbiota, with reported relative abundances ranging from approximately 0.5% and 5%[46]. It has been associated with several metabolic conditions, including overweight, obesity, type 2 diabetes, metabolic syndrome and hepatic steatosis[47]. Previous studies have suggested that *A. muciniphila* is linked to intestinal barrier protection in ALD, that ethanol exposure can reduce its abundance, and that *A. muciniphila* supplementation can improve experimental ALD phenotypes[48–50]. Furthermore, oral DHM administration has been reported to improve lipid metabolism and increase the relative abundance of *Akkermansia* in a mouse model of nonalcoholic steatohepatitis[51]. These findings are consistent with the microbiota-modulating potential of DHM. However, in our middle-aged alcohol-exposure model, DHM did not simply restore *Akkermansia* in a unidirectional manner. Instead, its effect appeared to depend on the alcohol-stressed ecological context. This discrepancy may reflect differences in disease model, host age, dietary background, mucus-layer status and microbial baseline ecology. Therefore, the bidirectional regulation of *Akkermansia* by DHM is not necessarily contradictory, but may reflect host-state-dependent ecological adaptation. Future studies using absolute abundance quantification, metagenomics and targeted functional assays will be needed to clarify the role of *Akkermansia* in DHM-mediated gut–liver axis remodeling.

Lachnospiraceae NK4A136 group also warrants attention. This taxon repeatedly appears in studies of age, metabolic intervention and gut barrier improvement. For example, it has been reported to show age-associated variation in mice[52], and changes in *Lachnospiraceae NK4A136 group* have been linked to improved barrier integrity in studies of spermidine intervention[53]. Members of the Lachnospiraceae family are often associated with short-chain fatty acid production and host metabolic health, but their functions are highly heterogeneous and should not be reduced to a simple beneficial label[54,55]. We therefore interpret *Lachnospiraceae NK4A136 group* as an ecological marker associated with middle-aged metabolic adaptation and intestinal barrier state, rather than as a confirmed functional mediator. Future metagenomic, SCFA and strain-level analyses will be needed to define its role in DHM-mediated ecological remodeling.

From an aging and disease perspective, the primary implication of this study is that different bioactive interventions may be suited to distinct pathological contexts and host physiological states. DHM preferentially modulates metabolic flexibility, epithelial adaptive turnover and context-dependent microbiota remodeling, whereas Silybin aligns with stress buffering, inflammatory lipid regulation and proteostasis support. These compounds are not simple substitutes; rather, they exhibit complementary adaptive profiles. This is consistent with the broader geroscience concept that intervention responses are shaped by host age, physiological resilience and disease context, rather than by a single therapeutic endpoint[12–15]. Future age-stratified intervention design for alcohol-associated liver injury should therefore account for host age, drinking status, metabolic phenotype and microbial ecology. This study provides a conceptual foundation for developing age-stratified bioactive intervention strategies for middle-aged populations at risk of ALD.

Several limitations should be considered. First, the multi-omics data define coherent association networks but do not establish causality. *Sgk1*, *Rhobtb1*, *Akkermansia* and *Lachnospiraceae NK4A136 group* should currently be considered candidate mechanistic nodes rather than confirmed direct targets. Second, the 16S sample size was limited, meaning genus-level findings should be interpreted as ecological trends. Third, the absence of targeted metabolomics, SCFA quantification, intestinal permeability testing or microbiota transplantation precludes definitive claims about microbiota-mediated protection. Fourth, DHM and Silybin differ in pharmacokinetics and bioavailability, which may partially explain their divergent response patterns. Finally, validation in female cohorts, diverse age strata and longer alcohol-exposure models will be required in future studies.

Overall, this study proposes a systems-level model for bioactive intervention in aging-associated liver vulnerability. Under middle-aged alcohol exposure, DHM and Silybin both mitigated alcohol-induced liver injury phenotypes, but were associated with distinct adaptive pathways. DHM was associated with adaptive metabolic–epithelial–microbial remodeling, including energy-metabolic adaptation, detoxification-associated metabolic remodeling, recovery of jejunal epithelial renewal programs and context-dependent microbial regulation. Silybin was aligned with stress-buffering and inflammatory homeostasis, including ER stress attenuation, inflammatory lipid signaling regulation, immune-associated pathway remodeling and microbial ecological rebalancing. Ultimately, these findings

challenge the conventional paradigm of natural products as generic antioxidant hepatoprotectants. These findings support a shift from reductionist, single-endpoint evaluation toward age-stratified intervention designs that account for host age, baseline metabolic state and the dynamic ecology of the gut–liver axis. Notably, the DHM-associated metabolic–epithelial–microbial adaptation highlights its potential as a candidate bioactive strategy for reinforcing gut–liver axis resilience under middle-aged alcohol-associated stress.

Methods

Population-based dataset analysis

GBD 2023 data analysis

Population-level burden data for alcohol-associated liver disease (ALD) were obtained from the Global Burden of Disease Study 2023 (GBD 2023). Data on the global burden of alcohol-associated liver disease from 2019 to 2023 were extracted from the GBD Results Tool to analyze age-specific prevalence trends. ALD-related burden was defined as alcohol-attributable liver disease burden and mainly included alcohol-associated cirrhosis and alcohol-associated liver cancer. Analyses used both-sex estimates and were stratified according to standard GBD age groups. The primary effect measure was prevalence per 100,000 population with 95% uncertainty intervals (UI). To reduce the influence of single-year fluctuation on age-trend interpretation, data from 2019 to 2023 were averaged before visualization, and cubic spline interpolation was used to smooth age-specific prevalence curves. Data processing, statistical analysis and plotting were performed in R, mainly using the tidyverse and ggplot2 packages.

NHANES data analysis

Public data from the National Health and Nutrition Examination Survey (NHANES) were used for cross-sectional analysis. Because the NHANES 2019–2020 cycle was discontinued early owing to the COVID-19 pandemic, we used the NCHS-released 2017–March 2020 pre-pandemic file with official sampling weights and further combined it with the August 2021–August 2023 cycle. This combined dataset was used to evaluate associations between drinking exposure and liver biochemical markers across age strata. The 2017–March 2020 pre-pandemic file comprises the 2017–2018 cycle and the incomplete 2019–March 2020 cycle. NCHS provides corresponding public-use weights, strata and primary sampling units (PSU) for this file. The August 2021–August 2023 cycle represents an independent post-pandemic NHANES cycle and can be combined with previous cycles according to CDC/NCHS analytic guidance.

Participants were included if they were ≥18 years of age and had complete serum liver enzyme data (ALT, AST and GGT), alcohol intake information and key covariate data. Individuals with positive hepatitis B or hepatitis C test results and those missing key variables were excluded. Daily alcohol intake was calculated from NHANES alcohol questionnaire and/or dietary recall data and converted into grams of pure alcohol per day (g/day). Participants were classified as light drinkers (≤14 g/day), moderate

drinkers (14–40 g/day) or heavy drinkers (>40 g/day). Age strata were defined as 18–34, 35–49, 50–64 and ≥65 years.

All analyses accounted for the complex multistage NHANES sampling design, including sampling weights, strata and PSU. For analyses combining the 2017–March 2020 pre-pandemic file with the August 2021–August 2023 cycle, weights were adjusted across cycles according to CDC/NCHS analytic guidance, and survey design variables were included in the models. Survey-weighted generalized linear models were used to evaluate associations of age stratum and drinking intensity with serum ALT, AST and GGT levels, with adjustment for sex, race/ethnicity and other covariates. To compare dose-response relationships between alcohol intake and GGT across age strata, age-stratified survey-weighted linear regression was used to analyze associations between daily alcohol intake and GGT.

Animals and experimental design

Male C57BL/6J mice at 11–12 months of age were purchased from Zhejiang Vital River Laboratory Animal Technology Co., Ltd. Mice were housed in a specific pathogen-free animal facility at the Laboratory Animal Center of Peking University Shenzhen Graduate School. Environmental temperature was maintained at 22 ± 2°C, relative humidity at 50 ± 10%, with a 12 h light/dark cycle. Mice were housed 3–5 per cage and had free access to water. After 7 days of acclimation, mice were randomly assigned by body weight to five groups: Control, DHM alone, EtOH model, EtOH + DHM and EtOH + Silybin. Histopathological quantification, image analysis and omics data analysis were performed under blinded conditions whenever possible. All animal procedures were approved by the Animal Ethics Committee of Peking University Shenzhen Graduate School (approval number AP20250521-01). All animal experiments and related methods were reported in accordance with the ARRIVE guidelines.

Alcohol-associated liver injury model

A modified Lieber–DeCarli liquid diet was used to establish a chronic alcohol-associated liver injury model. Lieber–DeCarli liquid diet was purchased from Jiangsu Xietong Pharmaceutical Bioengineering Co., Ltd. Because mice at 11–12 months of age have relatively low tolerance to alcohol exposure, the classic NIAAA alcohol feeding model [19] was moderately adapted for this study. The alcohol-feeding and intervention phase lasted 23 days, whereas survival was monitored throughout the 34-day experimental period. During the alcohol modeling phase, ethanol concentration was gradually increased from 1% (v/v) to 4% (v/v) on days 1–4 and maintained at 4% (v/v) on days 5–18. Control and DHM-alone groups received isocaloric maltodextrin instead of ethanol and were pair-fed to correct for differences in food intake. Fresh liquid diet was replaced daily between 15:00 and 17:00, and food intake was recorded. Humane endpoint criteria included body weight loss exceeding 20%, persistent hunched posture, marked reduction in activity, inability to eat or drink normally, or other signs of severe distress. Before the experimental endpoint, mice were fasted for 6 h. Blood was collected by cardiac puncture under

isoflurane anesthesia, followed by cervical dislocation and collection of liver, kidney, jejunum and fecal samples.

Dihydromyricetin and Silybin administration

Dihydromyricetin (DHM, purity ≥98%) was purchased from Yuanye Bio-Technology. Silybin (purity ≥98%) was purchased from Aladdin. DHM was administered at 200 mg/kg/day, and Silybin was administered at 100 mg/kg/day. Both compounds were suspended in 0.5% sodium carboxymethylcellulose (CMC-Na) solution and administered once daily by oral gavage at 15:00, with a dosing volume of 10 mL/kg. Drug suspensions were freshly prepared every 3 days and stored at 4°C protected from light.

Survival, body weight, food intake and behavioral assessments

Mice were inspected daily throughout the experiment, and deaths were recorded for Kaplan–Meier survival analysis. Body weight was measured every 2 days, and food intake was recorded daily. Grip strength was measured using a Xinruan animal grip strength meter. Each mouse was tested three consecutive times, and the mean value was used as the final grip strength. The open-field test was performed in a 40 × 40 × 40 cm white plastic arena under approximately 50 lux illumination. After 5 min of acclimation, free movement was recorded for 10 min. Total distance, center-zone residence time and movement trajectories were analyzed using ANY-maze software.

Serum biochemical assays and histological analysis

Blood samples were kept at room temperature for 30 min and centrifuged at 3500 rpm for 15 min. Serum was collected and stored at −80°C. Serum AST, ALT and TG levels were measured using an automated biochemical analyzer (Medicalsystem MS480). Left liver lobes were fixed in 4% paraformaldehyde (PFA), dehydrated through a sucrose gradient, cryosectioned at 8 μm and stained with Oil Red O. Right liver lobes and kidney tissues were fixed in 4% PFA, paraffin-embedded, sectioned and stained with H&E. Paraffin sectioning and H&E staining were performed by BioMed World Pathology Technology Service Co., Ltd. Stained sections were imaged using a Leica DM750 microscope. Five random non-overlapping fields were selected from each section for quantitative analysis. Oil Red O-positive area, steatosis area and related histological indices were quantified using ImageJ software.

Liver and jejunum RNA sequencing

RNA-seq library preparation, sequencing and preliminary bioinformatics analyses of liver and jejunum tissues were performed by Tsingke Biotechnology Co., Ltd. Briefly, total RNA was extracted from tissues using TRIzol reagent. RNA concentration was measured with a NanoDrop 2000, and RNA integrity was assessed using an Agilent 2100 and LabChip GX. Samples were required to meet quality control criteria of total RNA amount ≥ 2 μg, concentration ≥ 40 ng/μL and RIN ≥ 7.0. Libraries were constructed using an mRNA capture strategy. Poly-A-tailed mRNA was first enriched with Oligo(dT) magnetic beads and fragmented into short fragments. Double-stranded cDNA was synthesized from fragmented mRNA, followed by end repair, A-tailing, adapter ligation, size selection and PCR amplification. Products were denatured and circularized to generate single-stranded circular DNA (ssCir DNA), which was then amplified by rolling circle amplification (RCA) to form DNA nanoballs (DNBs). Sequencing was performed on the DNBSEQ-T7 high-throughput sequencing platform. Raw data were quality controlled using fastp (v0.20.1). Clean data were obtained by removing adapters and low-quality sequences with parameters -q 20 -l 100 -n 10. Clean data were aligned to the mouse reference genome GRCm39 (version 112) using HISAT2 (v2.2.1). StringTie (v2.0.4) was used for initial transcript assembly, and gffcompare (v0.9.8) was used to assess transcript matching with reference annotation. Gene expression was quantified as FPKM values using the ballgown package. Differentially expressed genes (DEGs) were identified using thresholds of $|\log2FC| > 1.5$ and $P < 0.05$. Functional enrichment analyses included Gene Ontology (GO), KEGG pathway enrichment and gene set enrichment analysis (GSEA). Bioinformatics analyses and visualization were performed using the Tsingke Cloud platform and R.

Untargeted serum metabolomics

Untargeted serum metabolomics was performed by Novogene Co., Ltd., and data processing and analysis were conducted on the Novogene Cloud platform. Briefly, 100 μL serum was mixed with 400 μL precooled methanol for protein precipitation, vortexed and centrifuged at low temperature. The supernatant was collected for LC-MS analysis. Quality control (QC) samples were prepared by pooling equal volumes from all experimental samples and were used to assess analytical stability and batch effects. Metabolite separation was performed on a Q Exactive™ HF-X ultra-high-resolution mass spectrometry platform (Thermo Fisher Scientific). Mass spectrometry was conducted in positive and negative ion modes. Raw data were converted to mzXML format using ProteoWizard, followed by peak extraction, peak quantification and retention-time correction using XCMS. Metabolite identification was based on Novogene's in-house standard database NovoMetDB-UM-V1.0 and followed internationally accepted Level 1 identification criteria, namely reference-standard MS/MS spectra plus MS1, MS2 and RT matching. MetaX was used for log transformation and normalization of quantitative data. DAMs were identified using thresholds of VIP > 1.0, fold change (FC) > 1.5 or <0.667, and $P < 0.05$. Orthogonal partial least-squares discriminant analysis (OPLS-DA) and 200 permutation tests were used to evaluate model stability and reduce overfitting. Final visualization and statistical summaries were completed in R (Version 4.5.1) and GraphPad Prism (version 10.6.0).

RT-qPCR validation

Approximately 30 mg of mid-jejunal tissue was gently rinsed with precooled saline to remove luminal contents and immediately snap-frozen in liquid nitrogen. RNA was extracted using an RNA extraction kit (Vazyme RC113), and cDNA was synthesized using the HiScript III All-in-one RT SuperMix Perfect for qPCR kit (Vazyme R433). Amplification was performed on a QuantStudio 3 system using a SYBR Green qPCR kit (Q713). *Gapdh* was used as the internal reference gene, and relative expression was calculated using the $2^{-\Delta\Delta Ct}$ method. Primer sequences are listed in **Table 1**.

Table 1. Primer sequences for RT-qPCR

Primer name	Forward Sequences (5'-3')	Reverse Sequences (5'-3')
Gapdh	TGGCCTTCCGTGTTCCTAC	GAGTTGCTGTTGAAGTCGCA
Rhobtb1	ACCACCCTGACACAGTACCAG	CGAAAGCCTTCCACGTCCG
Sgk1	GTGTCAATCATGCCTGGGTGA	CTCCAACCCTCACGCCAAAC
Cdkn1a	GTGTCTGAGCGGCCTGAAG	GGGCACTTCAGGGTTTTCTCTTG
Reg3g	CCCATCTTCACGTAGCAGCTG	CAAGATGTCCTGAGGGCCTCT

16S rRNA sequencing and microbiome analysis

Fresh fecal samples were collected at the experimental endpoint, immediately snap-frozen in liquid nitrogen and stored at −80°C. 16S rRNA sequencing was performed by Novogene Co., Ltd. Total fecal genomic DNA was extracted using the QIAamp Fast DNA Stool Mini Kit. The V3–V4 variable region of the bacterial 16S rRNA gene was amplified using primers 341F (5'-CCTAYGGGRBGCASCAG-3') and 806R-mod (5'-GGACTACNNGGGTATCTAAT-3'). The 25 μL PCR reaction contained 15 μL Phusion® High-Fidelity PCR Master Mix (New England Biolabs), 0.2 μM primers and approximately 10 ng template DNA. PCR products were checked by 2% agarose gel electrophoresis and purified using magnetic beads. Libraries were prepared using the TruSeq® DNA PCR-Free Sample Preparation Kit. After Qubit and Q-PCR quantification and library quality control, PE250 paired-end sequencing was performed on an Illumina NovaSeq 6000 platform. Data were processed using the QIIME2 pipeline (version 2022.2). Raw reads were subjected to adapter trimming and quality control, followed by denoising, merging and chimera removal using the DADA2 plugin to obtain high-resolution amplicon sequence variants (ASVs). Taxonomic annotation was performed using the classify-sklearn algorithm against the SILVA 138 database. To reduce the influence of sequencing-depth differences, all samples were rarefied to the minimum effective sequencing depth. Alpha diversity was assessed using the Simpson index. Beta diversity was calculated based on Bray–Curtis distance and visualized by principal coordinates analysis (PCoA). SIMPER analysis was performed using the vegan package in R to evaluate species contributions

to between-group dissimilarity. Differential microbial taxa were identified using LEfSe (v1.0), with an LDA score threshold > 2.0.

Statistical analysis

Except for analyses built into omics platforms, statistical analyses were mainly performed using GraphPad Prism 10.6 and R. Data normality was first assessed using the Shapiro-Wilk test. Normally distributed continuous variables with homogeneous variances were analyzed using one-way ANOVA followed by the Bonferroni post hoc test for selected comparisons. Non-normally distributed data were analyzed using the Kruskal–Wallis test with Dunn's multiple-comparison post hoc test. Survival curves were generated using the Kaplan–Meier method and compared using the Gehan–Breslow–Wilcoxon test. Microbial relative abundance data were analyzed using non-parametric tests. All tests were two-sided, and $P < 0.05$ was considered statistically significant. Unless otherwise stated, data are presented as mean ± SEM.

Declarations

Data Availability

All datasets generated or analyzed in this study are available from the corresponding author upon reasonable request.

Acknowledgements

This study was supported by the Guangdong Science and Technology Program (2024B1111130001), the Shenzhen Science and Technology Program (KJZD20240903102703005) and (JCYJ20240813094515020), and a Sirio Pharma Co., Ltd. project (SA25100479).

Author contributions

JL: Conceptualization, Experiment validation, Data curation, Writing – original draft, review and editing. XZ: Conceptualization, Writing – review and editing. LL, XJ, YZ, CH: Experiment validation and Data curation. DY: Data curation. QS: Writing – review and editing. XW: Supervision, Writing – review and editing. JKZ: Funding acquisition, Supervision, Writing – review and editing, YXL: Conceptualization, Funding acquisition, Supervision, Writing – original draft, review and editing.

Competing interests

The authors declare no competing interests.

References

1. Devarbhavi, H. *et al.* Global burden of liver disease: 2023 update. *Journal of Hepatology* **79**, 516–537 (2023).
2. Åberg, F., Jiang, Z. G., Cortez-Pinto, H. & Männistö, V. Alcohol-associated liver disease—Global epidemiology. *Hepatology* **80**, 1307–1322 (2024).
3. Mackowiak, B., Fu, Y., Maccioni, L. & Gao, B. Alcohol-associated liver disease. *J Clin Invest* **134**, (2024).
4. Mandrekar, P. & Mandal, A. Pathogenesis of Alcohol-Associated Liver Disease. *Clinics in Liver Disease* **28**, 647–661 (2024).
5. Danpanichkul, P. *et al.* Global and regional burden of alcohol-associated liver disease and alcohol use disorder in the elderly. *JHEP Reports* **6**, 101020 (2024).
6. Raya Tonetti, F. *et al.* Gut-liver axis: Recent concepts in pathophysiology in alcohol-associated liver disease. *Hepatology* **80**, 1342–1371 (2024).
7. Bajaj, J. S. Alcohol, liver disease and the gut microbiota. *Nat Rev Gastroenterol Hepatol* **16**, 235–246 (2019).
8. Shen, H., Liangpunsakul, S., Iwakiri, Y., Szabo, G. & Wang, H. Immunological mechanisms and emerging therapeutic targets in alcohol-associated liver disease. *Cell Mol Immunol* **22**, 1190–1204 (2025).
9. An, L. *et al.* The Role of Gut-Derived Lipopolysaccharides and the Intestinal Barrier in Fatty Liver Diseases. *Journal of Gastrointestinal Surgery* **26**, 671–683 (2022).
10. Yang, Y. & Schnabl, B. Gut Bacteria in Alcohol-Associated Liver Disease. *Clinics in Liver Disease* **28**, 663–679 (2024).
11. Ren, R. *et al.* Aging exaggerates acute-on-chronic alcohol-induced liver injury in mice and humans by inhibiting neutrophilic sirtuin 1-C/EBPα-miRNA-223 axis. *Hepatology* **75**, 646–660 (2021).
12. Bellamkonda, R. *et al.* Effect of aging on the development and progression of alcohol-associated liver disease. *Alcohol, Clinical and Experimental Research* **49**, 1412–1423 (2025).
13. Kroemer, G. *et al.* From geroscience to precision geromedicine: Understanding and managing aging. *Cell* **188**, 2043–2062 (2025).
14. Salazar, A. M., Aparicio, R., Clark, R. I., Rera, M. & Walker, D. W. Intestinal barrier dysfunction: an evolutionarily conserved hallmark of aging. *Disease Models & Mechanisms* **16**, dmm049969 (2023).
15. Kim, H.-H. & Dixit, V. D. Metabolic regulation of immunological aging. *Nat Aging* **5**, 1425–1440 (2025).
16. McMahan, R. H. *et al.* A novel murine model of multi-day moderate ethanol exposure reveals increased intestinal dysfunction and liver inflammation with age. *Immun Ageing* **18**, 37 (2021).
17. Janilkarn-Urena, I. *et al.* Dihydromyricetin supplementation improves ethanol-induced lipid accumulation and inflammation. *Front. Nutr.* **10**, 1201007 (2023).

18. Abenavoli, L. *et al.* Milk thistle (Silybum marianum): A concise overview on its chemistry, pharmacological, and nutraceutical uses in liver diseases. *Phytotherapy Research* **32**, 2202–2213 (2018).
19. Bertola, A., Mathews, S., Ki, S. H., Wang, H. & Gao, B. Mouse model of chronic and binge ethanol feeding (the NIAAA model). *Nat Protoc* **8**, 627–637 (2013).
20. Jackson, S. J. *et al.* Does age matter? The impact of rodent age on study outcomes. *Lab Anim* **51**, 160–169 (2016).
21. Gao, B. & Bataller, R. Alcoholic Liver Disease: Pathogenesis and New Therapeutic Targets. *Gastroenterology* **141**, 1572–1585 (2011).
22. Jiang, Y. *et al.* Alcohol Metabolizing Enzymes, Microsomal Ethanol Oxidizing System, Cytochrome P450 2E1, Catalase, and Aldehyde Dehydrogenase in Alcohol-Associated Liver Disease. *Biomedicines* **8**, 50 (2020).
23. Lu, Y. & Cederbaum, A. I. CYP2E1 and oxidative liver injury by alcohol. *Free Radical Biology and Medicine* **44**, 723–738 (2008).
24. Silva, J. *et al.* Dihydromyricetin Protects the Liver via Changes in Lipid Metabolism and Enhanced Ethanol Metabolism. *Alcohol Clin Exp Res* **44**, 1046–1060 (2020).
25. Jackson, K. G., Way, G. W., Zeng, J., Lipp, M. K. & Zhou, H. The Dynamic Role of Endoplasmic Reticulum Stress in Chronic Liver Disease. *The American Journal of Pathology* **193**, 1389–1399 (2023).
26. Ramirez, T. *et al.* Insulin Resistance, Ceramide Accumulation and Endoplasmic Reticulum Stress in Experimental Chronic Alcohol-Induced Steatohepatitis. *Alcohol and Alcoholism* **48**, 39–52 (2012).
27. Sahin, E., Bagci, R., Bektur Aykanat, N. E., Kacar, S. & Sahinturk, V. Silymarin attenuated nonalcoholic fatty liver disease through the regulation of endoplasmic reticulum stress proteins GRP78 and XBP-1 in mice. *J Food Biochem* **44**, e13194 (2020).
28. Zhang, B. *et al.* Silybin inhibits NLRP3 inflammasome assembly through the NAD+/SIRT2 pathway in mice with nonalcoholic fatty liver disease. *The FASEB Journal* **32**, 757–767 (2018).
29. Wu, J. *et al.* Silybin regulates P450s activity by attenuating endoplasmic reticulum stress in mouse nonalcoholic fatty liver disease. *Acta Pharmacol Sin* **44**, 133–144 (2022).
30. Pearce, D. SGK1 Regulation of Epithelial Sodium Transport. *Cell Physiol Biochem* **13**, 13–20 (2003).
31. Lang, F., Strutz-Seebohm, N., Seebohm, G. & Lang, U. E. Significance of SGK1 in the regulation of neuronal function. *J Physiol* **588**, 3349–3354 (2010).
32. Ahsan, M. K. *et al.* Loss of Serum Glucocorticoid-Inducible Kinase 1 SGK1 Worsens Malabsorption and Diarrhea in Microvillus Inclusion Disease (MVID). *JCM* **11**, 4179 (2022).
33. Balla, T. Phosphoinositides: Tiny Lipids With Giant Impact on Cell Regulation. *Physiological Reviews* **93**, 1019–1137 (2013).
34. Fang, S. *et al.* RhoBTB1 reverses established arterial stiffness in angiotensin II–induced hypertension by promoting actin depolymerization. *JCI Insight* **7**, e158043 (2022).

35. Mukohda, M. *et al.* RhoBTB1 protects against hypertension and arterial stiffness by restraining phosphodiesterase 5 activity. *J Clin Invest* **129**, 2318–2332 (2019).
36. Fang, S. & Sigmund, C. D. PPARγ and RhoBTB1 in hypertension. *Current Opinion in Nephrology and Hypertension* **29**, 161–170 (2020).
37. Liu, C., Russell, R. M., Seitz, H. K. & Wang, X.-D. Ethanol enhances retinoic acid metabolism into polar metabolites in rat liver via induction of cytochrome P4502E1. *Gastroenterology* **120**, 179–189 (2001).
38. Clugston, R. D. & Blaner, W. S. The Adverse Effects of Alcohol on Vitamin A Metabolism. *Nutrients* **4**, 356–371 (2012).
39. Ferdouse, A. *et al.* Alcohol induced hepatic retinoid depletion is associated with the induction of multiple retinoid catabolizing cytochrome P450 enzymes. *PLoS ONE* **17**, e0261675 (2022).
40. Stevison, F., Jing, J., Tripathy, S. & Isoherranen, N. Role of Retinoic Acid-Metabolizing Cytochrome P450s, CYP26, in Inflammation and Cancer. *Adv Pharmacol* **74**, 373–412 (2015).
41. Melis, M., Tang, X.-H., Trasino, S. E. & Gudas, L. J. Retinoids in the Pathogenesis and Treatment of Liver Diseases. *Nutrients* **14**, 1456 (2022).
42. Marín, L., Miguélez, E. M., Villar, C. J. & Lombó, F. Bioavailability of Dietary Polyphenols and Gut Microbiota Metabolism: Antimicrobial Properties. *BioMed Research International* **2015**, 1–18 (2015).
43. Luca, S. V. *et al.* Bioactivity of dietary polyphenols: The role of metabolites. *Critical Reviews in Food Science and Nutrition* **60**, 626–659 (2019).
44. Alqudah, S. & Claesen, J. Mechanisms of gut bacterial metabolism of dietary polyphenols into bioactive compounds. *Gut Microbes* **16**, (2024).
45. Luo, Y. *et al.* Rational consideration of Akkermansia muciniphila targeting intestinal health: advantages and challenges. *npj Biofilms Microbiomes* **8**, 81 (2022).
46. Geerlings, S. Y., Kostopoulos, I., De Vos, W. M. & Belzer, C. Akkermansia muciniphila in the Human Gastrointestinal Tract: When, Where, and How? *Microorganisms* **6**, 75 (2018).
47. Cani, P. D., Depommier, C., Derrien, M., Everard, A. & de Vos, W. M. Akkermansia muciniphila: paradigm for next-generation beneficial microorganisms. *Nat Rev Gastroenterol Hepatol* **19**, 625–637 (2022).
48. Grander, C. *et al.* Recovery of ethanol-induced Akkermansia muciniphila depletion ameliorates alcoholic liver disease. *Gut* **67**, 891–901 (2017).
49. Derrien, M., Vaughan, E. E., Plugge, C. M. & de Vos, W. M. Akkermansia muciniphila gen. nov., sp. nov., a human intestinal mucin-degrading bacterium. *International Journal of Systematic and Evolutionary Microbiology* **54**, 1469–1476 (2004).
50. Sparfel, L., Ratodiarivony, S., Boutet-Robinet, E., Ellero-Simatos, S. & Jolivet-Gougeon, A. *Akkermansia muciniphila* and Alcohol-Related Liver Diseases. A Systematic Review. *Molecular Nutrition Food Res* **68**, (2023).

51. Miao, X., Luo, P., Liu, J., Wang, J. & Chen, Y. Dihydromyricetin ameliorated nonalcoholic steatohepatitis in mice by regulating the composition of serous lipids, bile acids and ileal microflora. *Lipids Health Dis* **22**, 112 (2023).
52. Kim, H.-J., Moon, C. M., Kang, J. L. & Park, E.-M. Aging effects on the diurnal patterns of gut microbial composition in male and female mice. *Korean J Physiol Pharmacol* **25**, 575–583 (2021).
53. Ma, L. *et al.* Spermidine improves gut barrier integrity and gut microbiota function in diet-induced obese mice. *Gut Microbes* **12**, 1832857 (2020).
54. Ćesić, D. *et al.* Association of Gut Lachnospiraceae and Chronic Spontaneous Urticaria. *Life* **13**, 1280 (2023).
55. Kim, C. H. Complex regulatory effects of gut microbial short-chain fatty acids on immune tolerance and autoimmunity. *Cell Mol Immunol* **20**, 341–350 (2023).

Figures

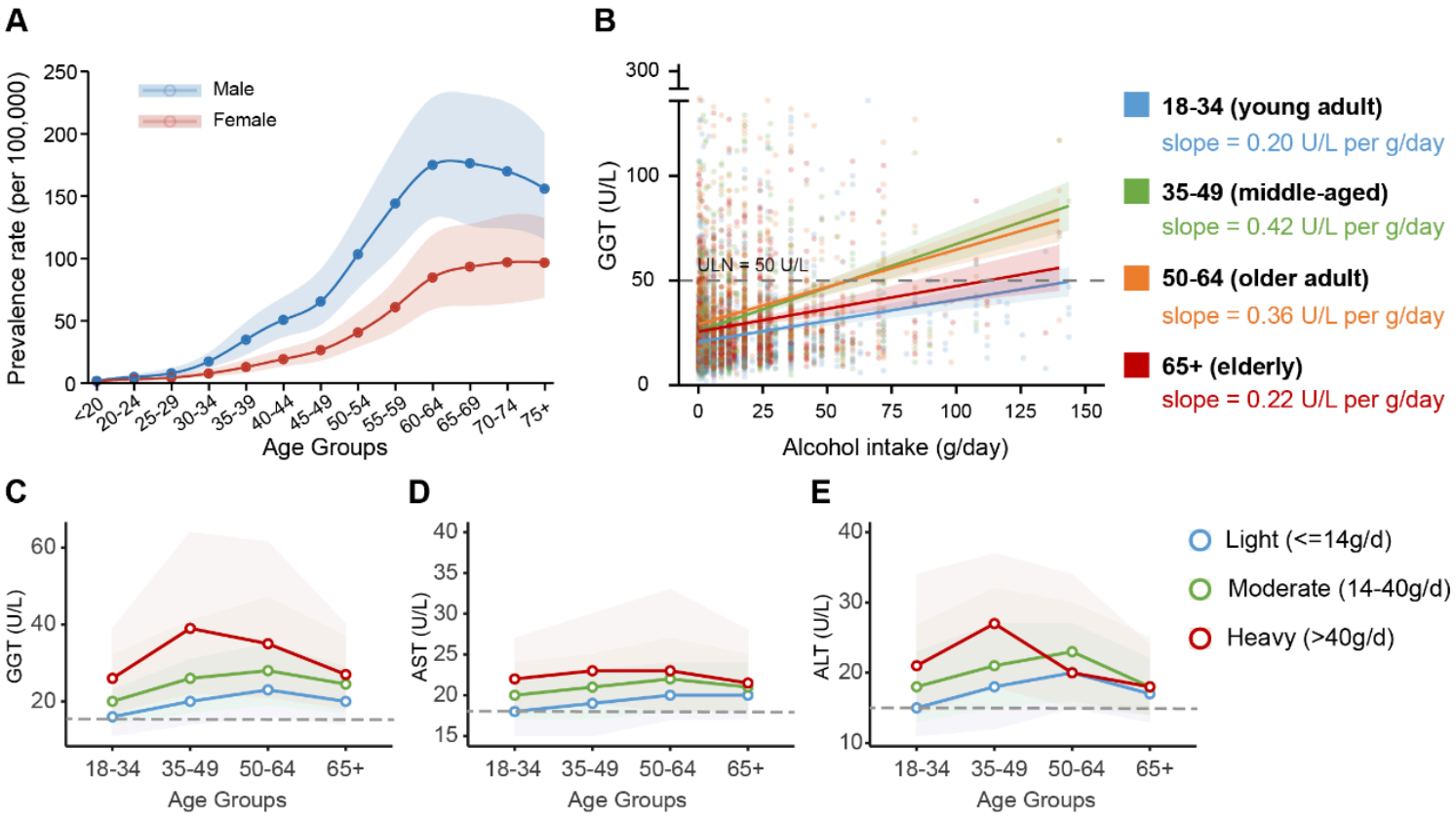


Figure 1

Population-based evidence identifies a middle-aged susceptibility window for alcohol-associated liver injury. (A) Global prevalence of alcohol-associated liver disease (ALD) across age groups and sexes based on GBD 2019–2023 estimates. Values represent prevalence rates per 100,000 population, and shaded bands indicate uncertainty intervals. **(B)** Age-stratified linear regression analysis between daily alcohol intake and serum GGT levels based on NHANES 2017–March 2020 pre-pandemic file and the

August 2021–August 2023 cycle. The dashed line indicates the upper limit of normal (ULN = 50 U/L). Colored lines indicate fitted regression trends across age strata. **(C–E)**Age-stratified trends of serum GGT **(C)**, AST **(D)** and ALT **(E)**levels across light, moderate and heavy drinking categories. Shaded bands denote the interquartile range (IQR). Blue, green and red lines represent light (≤14 g/day), moderate (14–40 g/day) and heavy (>40 g/day) drinkers, respectively.

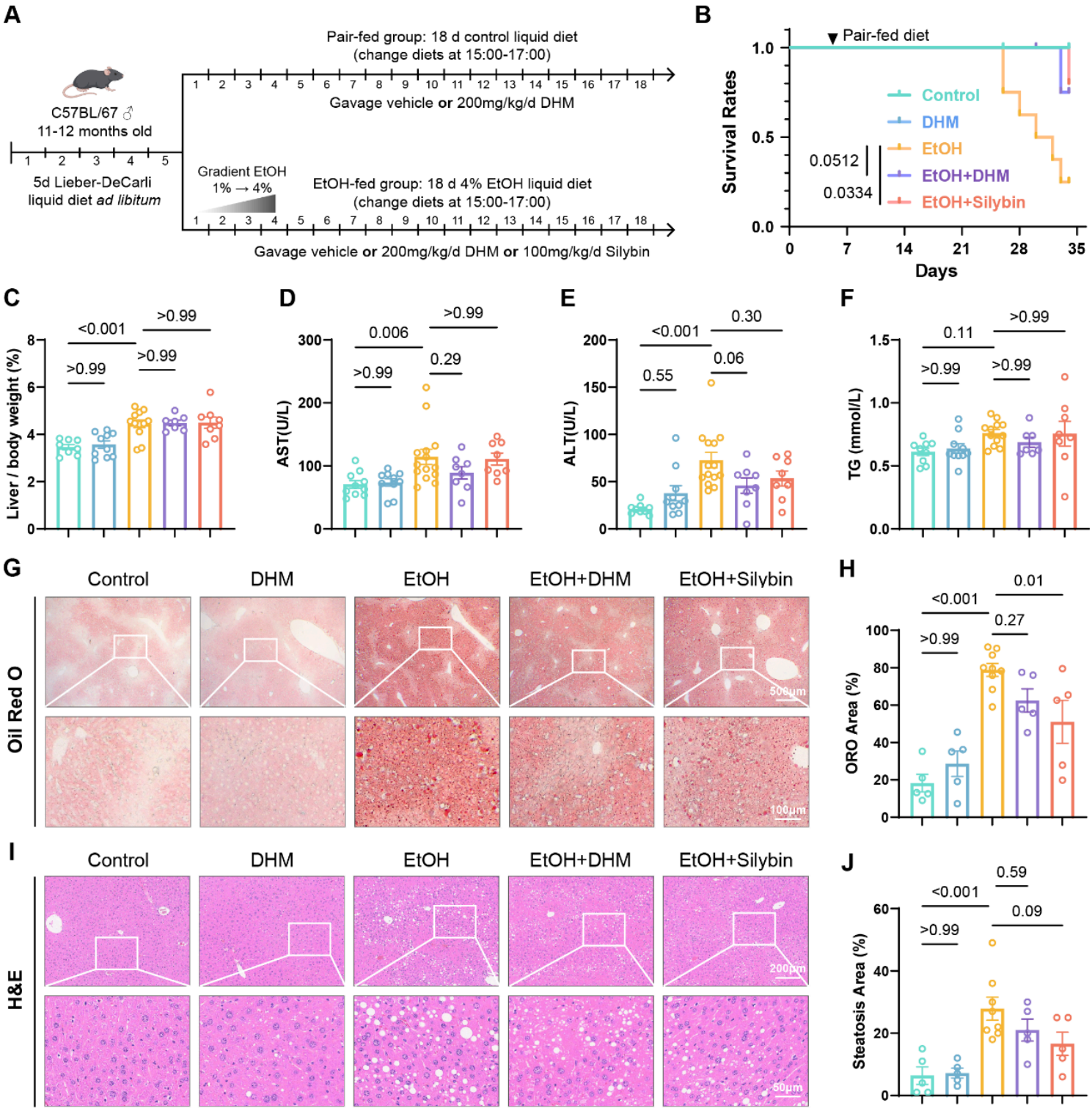


Figure 2

DHM and Silybin partially attenuate alcohol-associated liver injury in middle-aged mice. (A) Experimental design schematic. Male C57BL/6J mice aged 11–12 months were subjected to a modified Lieber–DeCarli alcohol-feeding protocol and treated with vehicle, DHM (200 mg/kg/day) or Silybin (100 mg/kg/day) by gavage. Pair-fed mice received an isocaloric control liquid diet. **(B)**Kaplan–Meier survival curves across experimental groups during the 34-day experimental period (n = 5–8 per group). P-values were determined using the Gehan test. **(C–F)** Liver/body weight ratio **(C)**, serum aspartate aminotransferase (AST) **(D)**, alanine aminotransferase (ALT) **(E)**and triglyceride (TG) levels **(F)** at the endpoint. **(G,H)** Representative Oil Red O staining images of liver sections **(G)** and quantification of Oil Red O-positive area **(H). (I,J)** Representative H&E staining images of liver sections **(I)** and quantification of hepatic steatosis area **(J)**. Scale bars are indicated in each image. Data are presented as mean ± SEM. Statistical significance was evaluated using one-way ANOVA followed by the Bonferroni post hoc test for selected comparisons.

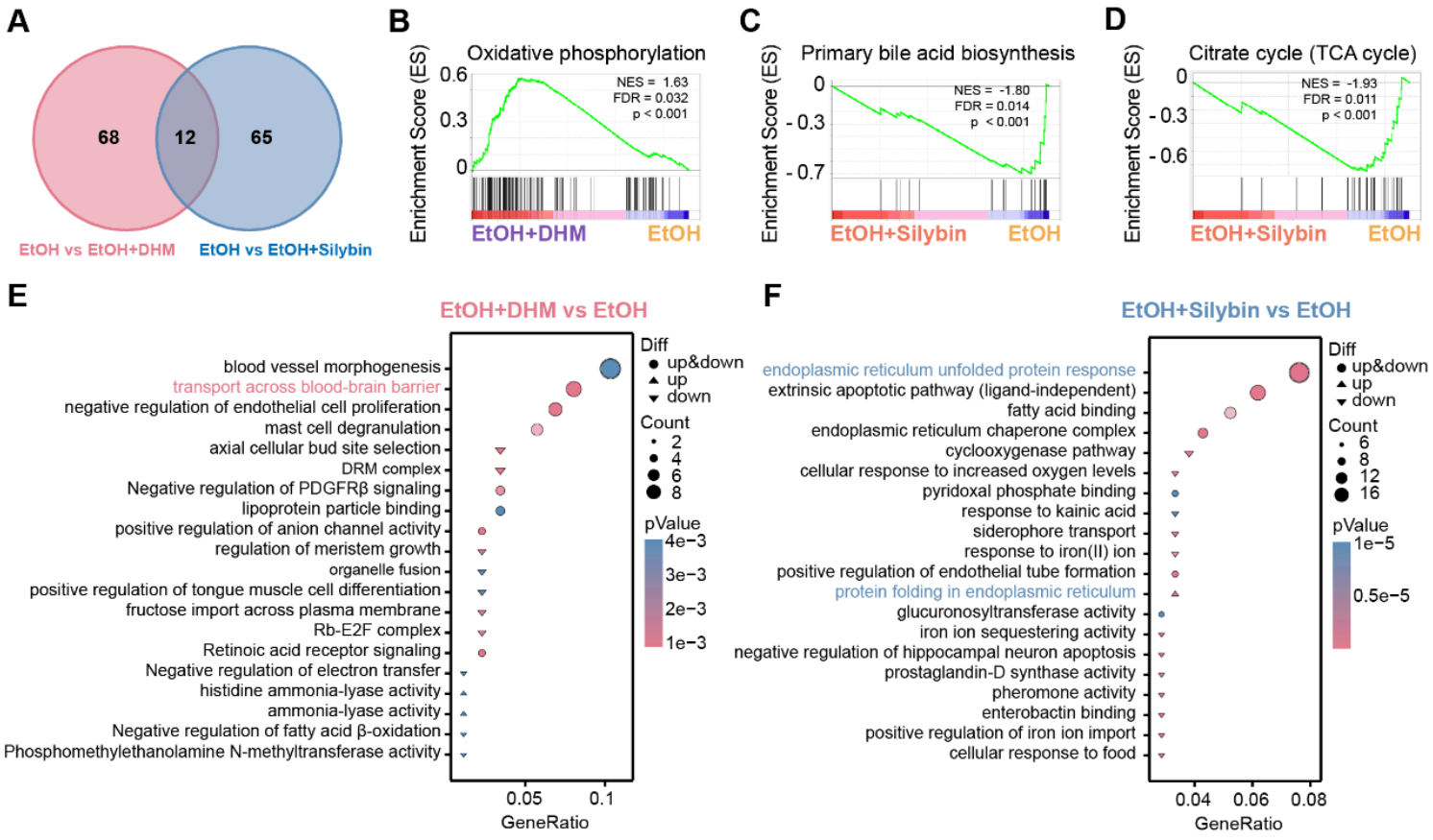


Figure 3

Distinct molecular signatures and functional enrichment of DHM and Silybin in middle-aged livers. (A) Venn diagram illustrating the overlap of differentially expressed genes (DEGs) in the liver for the EtOH+DHM vs. EtOH and EtOH+Silybin vs. EtOH comparisons. **(B–D)** Gene set enrichment analysis (GSEA) plots showing compound-associated metabolic modulation: DHM was associated with positive enrichment of oxidative phosphorylation **(B)**, whereas Silybin was associated with negative enrichment of primary bile acid biosynthesis **(C)** and the citrate cycle (TCA cycle) **(D)**. **(E,F)** Hierarchical Gene

Ontology (GO) dot plots for EtOH vs. EtOH+DHM **(E)** and EtOH vs. EtOH+Silybin **(F)**. DHM was associated with pathways related to blood vessel morphogenesis and transport across the blood–brain barrier, whereas Silybin was associated with the endoplasmic reticulum (ER) unfolded protein response and apoptotic signaling. NES, normalized enrichment score; FDR, false discovery rate.

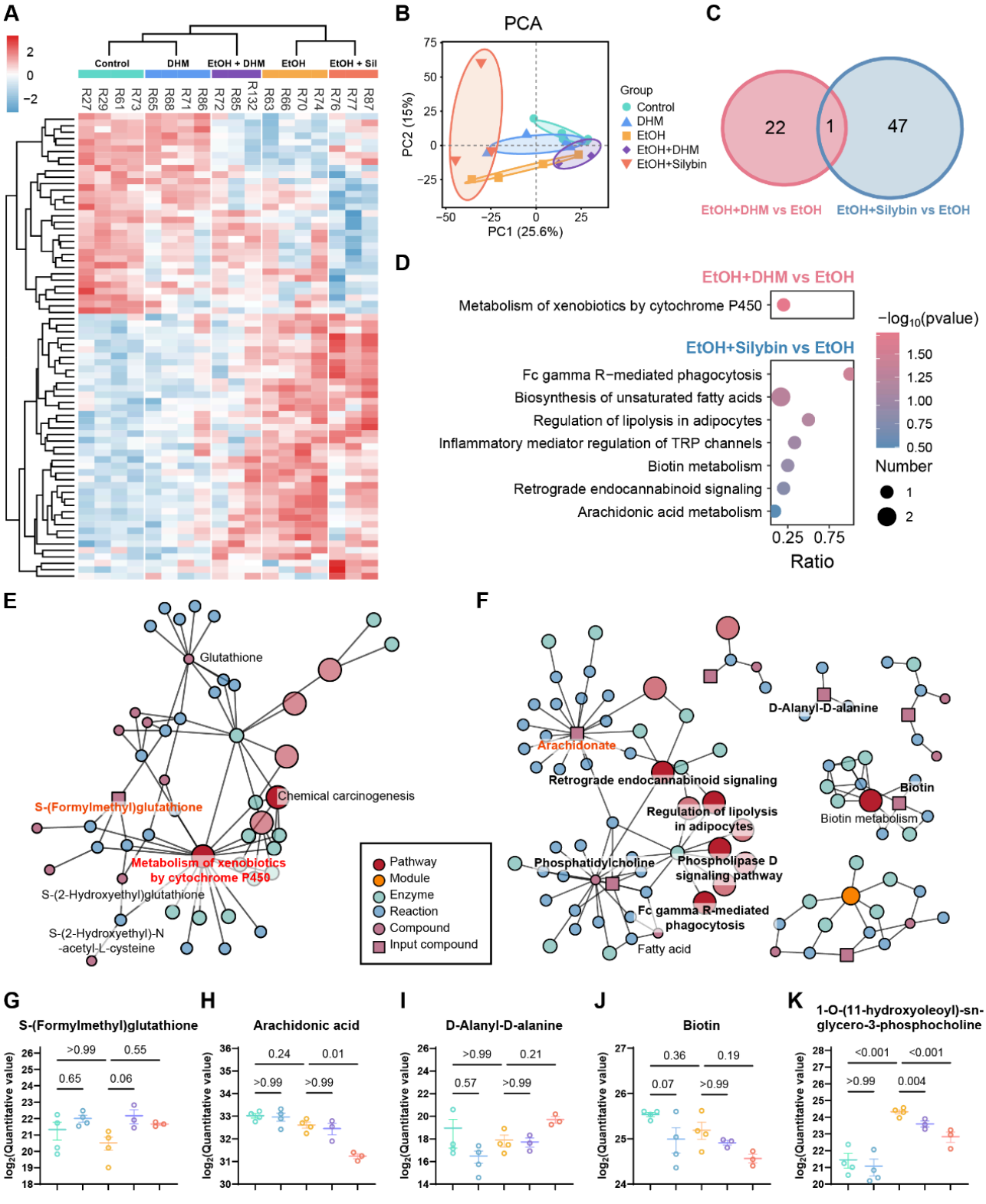


Figure 4

Serum metabolomic profiling identifies distinct metabolic signatures associated with DHM and Silybin intervention. (A,B) Global metabolic shifts visualized by hierarchical clustering heatmap **(A)** and principal component analysis (PCA) plot **(B)** of serum metabolites across five groups. **(C)** Venn diagram showing the overlap of DAMs identified in the EtOH+DHM vs. EtOH and EtOH+Silybin vs. EtOH comparisons. **(D)** KEGG pathway enrichment analysis of DAMs. DHM modulated metabolism of xenobiotics by cytochrome P450, whereas Silybin targeted multiple pathways including arachidonic acid metabolism and inflammatory mediator regulation of TRP channels. **(E,F)** Compound-pathway networks for DHM **(E)** and Silybin **(F)** groups. In the DHM network, S-(Formylmethyl)glutathione was highlighted as a major connected metabolite; arachidonate, D-Alanyl-D-alanine and biotin were highlighted in the Silybin-associated network. **(G–K)** Quantitative comparison of selected metabolic markers: S-(Formylmethyl)glutathione **(G)**, arachidonate **(H)**, D-Alanyl-D-alanine **(I)**, biotin **(J)** and 1-O-(11-hydroxyoleoyl)-sn-glycero-3-phosphocholine **(K)**. Data are expressed as $\log_2$(quantitative value) and presented as mean ± SEM. Statistical significance was evaluated using one-way ANOVA followed by the Bonferroni post hoc test for selected comparisons.

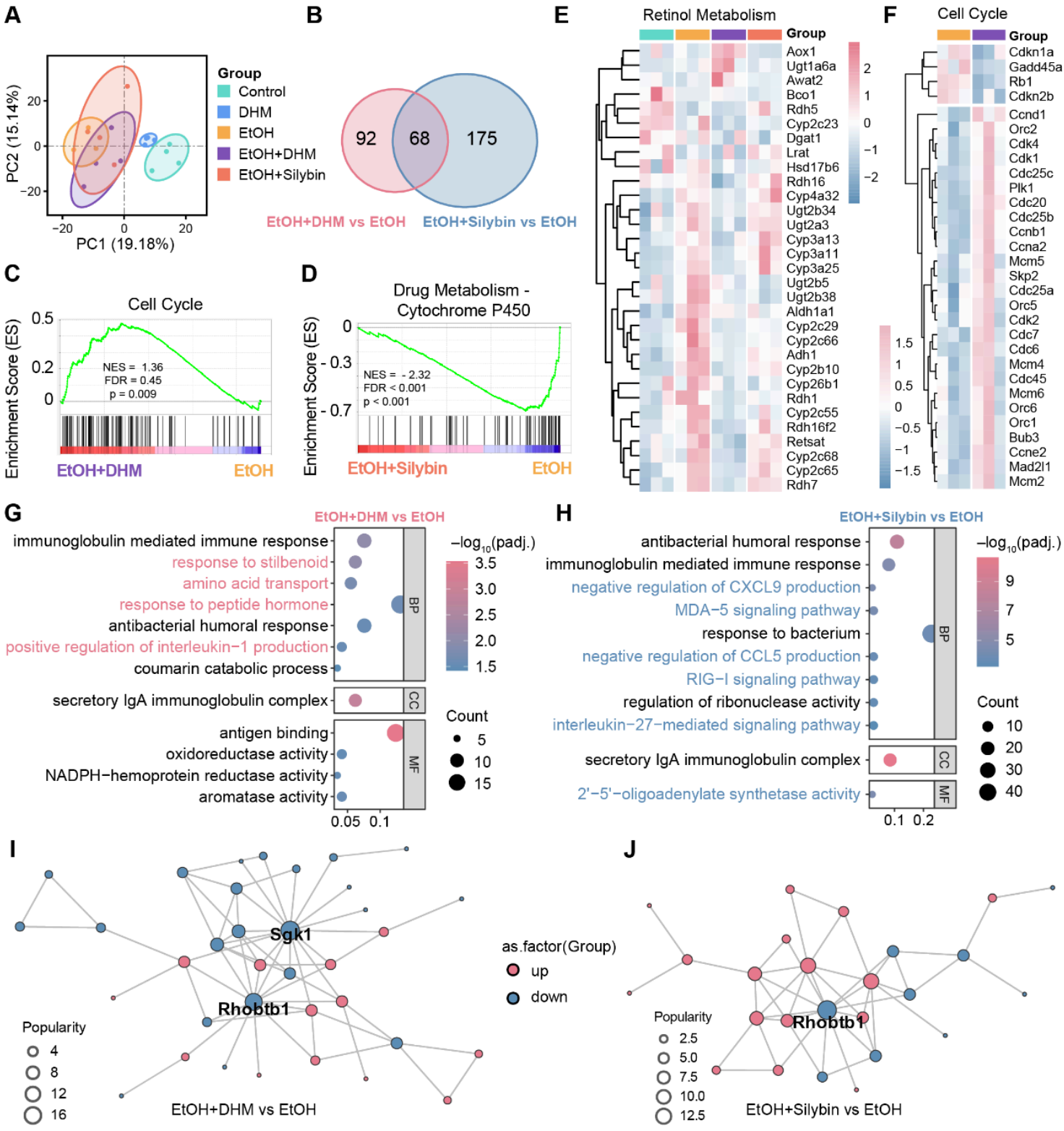


Figure 5

DHM and Silybin differentially regulate jejunal regenerative, metabolic and immune-associated transcriptional programs in middle-aged alcohol-fed mice. (A) Principal component analysis (PCA) of jejunal transcriptomic profiles among groups. **(B)** Venn diagram showing the overlap of differentially expressed genes (DEGs) between EtOH+DHM vs. EtOH and EtOH+Silybin vs. EtOH comparisons. **(C,D)** Gene set enrichment analysis (GSEA) showing enrichment of the cell cycle pathway in the EtOH+DHM

group **(C)**and suppression of the Drug metabolism – cytochrome P450 pathway in the EtOH+Silybin group **(D)**, compared with the EtOH group. **(E)** Heatmap showing representative genes involved in retinol metabolism across groups. **(F)**Heatmap showing representative genes associated with cell cycle regulation and DNA replication between EtOH and EtOH+DHM groups. **(G,H)** GO enrichment analysis of DEGs in EtOH+DHM vs. EtOH **(G)** and EtOH+Silybin vs. EtOH **(H)**comparisons. Biological process (BP), cellular component (CC) and molecular function (MF) categories are shown. **(I,J)** Gene interaction network analysis of DEGs in EtOH+DHM vs. EtOH **(I)** and EtOH+Silybin vs. EtOH **(J)**comparisons. Node size represents network connectivity, and node color indicates upregulated (pink) or downregulated (blue) genes. NES, normalized enrichment score; FDR, false discovery rate.

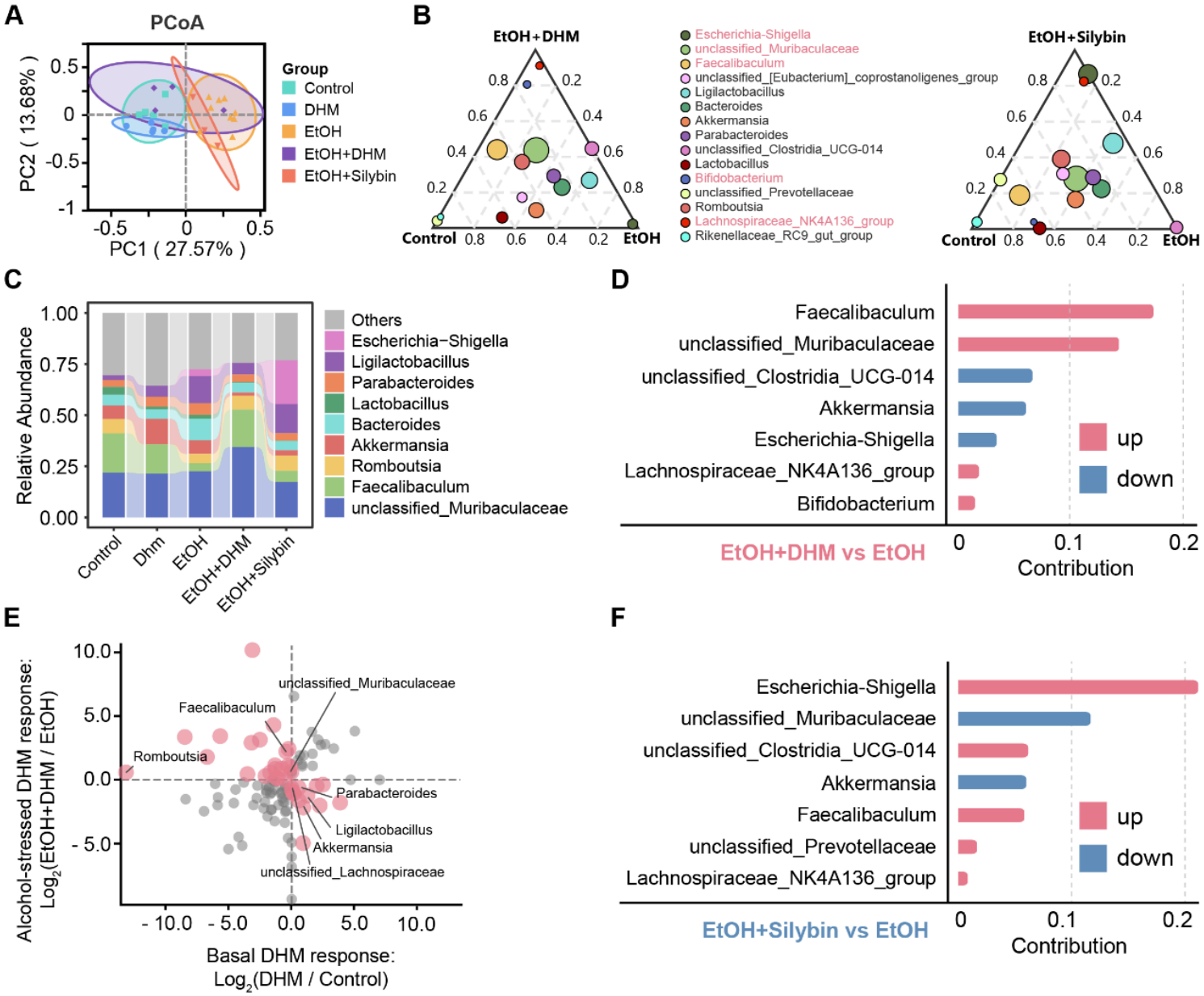


Figure 6

DHM and Silybin differentially remodel gut microbial ecology in middle-aged alcohol-fed mice. (A) Principal coordinates analysis (PCoA) of fecal microbial communities based on Bray–Curtis distance. **(B)** Ternary plots illustrating genus-level ecological redistribution across Control, EtOH and drug-treated groups. Each dot represents a bacterial genus, and the spatial position reflects its relative enrichment tendency among the three ecological states. **(C)** Genus-level relative abundance composition across experimental groups. Major genera are displayed, whereas low-abundance taxa are grouped as “Others”. **(D,F)** SIMPER analysis identifying representative contributing genera to community dissimilarity in EtOH+DHM vs. EtOH **(D)** and EtOH+Silybin vs. EtOH **(F)**. **(E)** Ecological response map depicting context-dependent microbial remodeling by DHM. The x-axis represents the basal DHM response under physiological conditions [Log_2(DHM/Control)], whereas the y-axis represents the alcohol-stressed DHM response [Log_2(EtOH+DHM/EtOH)]. Highlighted genera illustrate distinct response modes, including stress-specific enrichment, basal-specific enrichment and bidirectional remodeling patterns.

Supplementary Files

This is a list of supplementary files associated with this preprint. Click to download.

- SupplementaryinformationR1.docx
- image1.png